

Evaluation of Differentially Constrained Motion Models for Graph-Based Trajectory Prediction

Theodor Westny*, Joel Oskarsson†, Björn Olofsson‡, and Erik Frisk*

Abstract—Given their flexibility and encouraging performance, deep-learning models are becoming standard for motion prediction in autonomous driving. However, with great flexibility comes a lack of interpretability and possible violations of physical constraints. Accompanying these data-driven methods with differentially-constrained motion models to provide physically feasible trajectories is a promising future direction. The foundation for this work is a previously introduced graph-neural-network-based model, MTP-GO. The neural network learns to compute the inputs to an underlying motion model to provide physically feasible trajectories. This research investigates the performance of various motion models in combination with numerical solvers for the prediction task. The study shows that simpler models, such as low-order integrator models, are preferred over more complex, e.g., kinematic models, to achieve accurate predictions. Further, the numerical solver can have a substantial impact on performance, advising against commonly used first-order methods like Euler forward. Instead, a second-order method like Heun’s can greatly improve predictions.

I. INTRODUCTION

The unknown decisions of surrounding road users are a primary source of uncertainty in traffic situations. Similarly to how a human driver adapts its future trajectory based on anticipations of the environment—autonomous vehicles should be equipped with the ability to predict the future actions of other traffic participants in order to ensure safe and proactive operation. The *behavior prediction* task [1] encapsulates this problem of predicting the intention and future motion of surrounding traffic agents, and its importance as a research topic has grown significantly over the last decades.

Due to the considerable difficulty of hand-crafting models that can decode the social interactions between a time-varying number of traffic participants, learning-based approaches have offered useful adaptability, proving valuable in addressing these complex problems [2]. Despite their flexibility, however, learning-based methods exhibit certain limitations. First, unlike conventional state estimation, these methods often lack interpretability because of the numerous latent representations. More importantly, they rarely provide performance guarantees, rendering them less attractive in applications with stringent safety requirements. Recent research has proposed coupling (deep) data-driven models with differential constraints to address these issues within the scope of motion prediction.

This research was supported by the Strategic Research Area at Linköping-Lund in Information Technology (ELLIIT), the Swedish Research Council via the project *Handling Uncertainty in Machine Learning Systems* (contract number: 2020-04122), and the Wallenberg AI, Autonomous Systems and Software Program (WASP) funded by the Knut and Alice Wallenberg Foundation.

*Department of Electrical Engineering, Linköping University, Sweden.

†Department of Computer and Information Science, Linköping University, Sweden.

‡Department of Automatic Control, Lund University, Sweden.

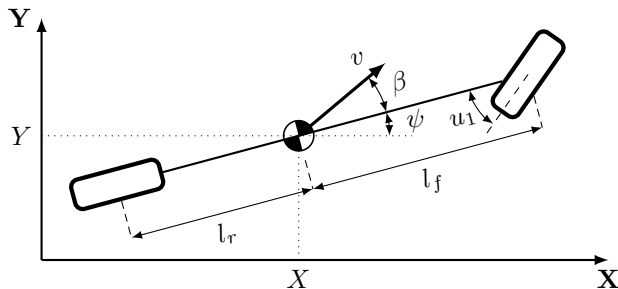


Fig. 1. Schematics of the kinematic single-track model with u_1 denoting the steering angle. Its use for motion prediction is interesting due to its connection and frequent use in autonomous planning and control applications [8].

The general idea is to have the learnable components of the model compute the inputs to an underlying motion model, thereby generating physically feasible outputs [3]–[6]. By drawing inspiration from target tracking [7], or model-based control [8], numerous formulations can be utilized for the motion prediction task, including various orders of integrators, non-holonomic constrained models or even Neural Ordinary Differential Equations (neural ODEs) [9].

Leveraging on our work in [6], this paper delves deeper into integrating deep graph-based networks with differentially-constrained motion models for trajectory prediction. The investigation focuses on the design of differential constraints, appropriate complexity class selection for heterogeneous traffic scenarios, and their impact on prediction and training performance. Furthermore, as numerical solvers are used to compute model states, the choice of integration methods can significantly influence the outcomes. In light of this, an investigation into the consequences of choosing various numerical solvers in combination with different motion models is conducted.

A. Contributions

The primary contributions of this paper are:

- An investigation into the properties of differentially constrained motion models across distinct complexity classes, illustrating their impact on overall model effectiveness.
- A study of the effects of diverse continuous-time integration techniques used in dynamic motion models, and their influence on training efficacy and prediction accuracy.

All investigations were performed based on the Graph Neural Network (GNN) architecture MTP-GO [6] for prediction performance using the *highD* [10] and *roundD* [11] data sets. Implementations are available online¹.

¹<https://github.com/westny/mtp-go>

II. RELATED WORK

The motion prediction problem can be found in many research fields, closely related to applications in state estimation and target tracking [2]. Predicting the future states of the ego-vehicle is useful for the development of active safety systems. In such applications, physics-based models are typically employed to obtain physically feasible predictions. In [12], a vehicle-dynamics model in combination with a Kalman filter is used to predict future position. In [13], the use of different physics-based vehicle models is presented for collision avoidance applications. An investigation on a range of curvilinear motion models [7] for vehicle tracking is presented in [14], illustrating the importance of appropriate model selection dependent on the application. While physics-based methods generalize well, they often simplify the true dynamics. One possibility entails using a grey-box approach to combine the physical model with learnable parts, for example, using Gaussian processes [15]. Combined with Kalman filtering, physics-based models are suitable for applications with short-term predictions. However, when the prediction horizon increases, assumptions on motion-model inputs become increasingly invalid, requiring time-varying input predictions conditioned on the current scene.

Recently, the motion prediction problem has been the target of learning-based research [1], [2]. Because of the temporal nature of the problem, several approaches have based their models on Recurrent Neural Networks (RNNs) [4], [5], [16]–[19] or more recently, Transformers [20], [21]. To utilize the spatial characteristics of the problem, these models are often integrated with Convolutional Neural Networks (CNNs) [18], [19], or GNNs [4], [5], [19], [22], [23]. A potential issue with complete black-box models aimed at predicting future motion is that model outputs can be physically infeasible. In [3], the use of a kinematic single-track model [8] is proposed for inclusion in the prediction model. The idea is to have a deep neural network compute the inputs to the motion model to generate kinematically feasible outputs. Trajectron++ [4] is a GNN-based method that does trajectory prediction by a recurrent generative model combined with model-based kinematic constraints. In the paper, a modified unicycle model is used to describe wheeled vehicles and a single-order integrator is used to describe pedestrians. STG-DAT [5] is a similarly structured model to that of Trajectron++. Similarly to [3], STG-DAT employs a kinematic single-track model in the prediction model. In [6], MTP-GO is proposed. The method uses an encoder–decoder model based on temporal GNNs to compute the motion model inputs. Instead of using predetermined motion constraints, the motion models are learned using neural ODEs.

III. PROBLEM FORMULATION

The trajectory prediction problem is formulated as estimating the probability distribution of the future positions of all agents $\nu \in \mathcal{V}_t$ currently in the scene for each time instant $t + 1, \dots, t + t_f$. The predicted mean future trajectory of an agent ν is a sequence $\hat{\mathbf{x}}_{t+1}^\nu, \dots, \hat{\mathbf{x}}_{t+t_f}^\nu$ of time-stamped positions in \mathbb{R}^2 . The forecasted trajectory is accompanied by an estimated state covariance $\mathbf{P}_{t+1}^\nu, \dots, \mathbf{P}_{t+t_f}^\nu$ used to represent

the prediction uncertainty. To provide dynamically feasible outputs, the future trajectories are computed using differentially constrained motion models f where

$$\dot{\mathbf{x}} = f(\mathbf{x}, \mathbf{u}), \quad (1)$$

and the input \mathbf{u} is the output of a deep neural network.

The two main research questions of this paper concern the formulation and integration of the motion model in the trajectory predictor. Possible model assumptions in (1) range from single integrators to kinematic models and neural ODEs. How this choice affects performance and training is a central research question. Since the models are formulated using differential equations, model states are retrieved using numerical integration methods. Therefore, the impact of the choice of numerical Ordinary Differential Equation (ODE) solver on training and prediction performance is researched. All investigations are performed based on a GNN architecture [6] and are evaluated using naturalistic driving data [10], [11].

IV. GRAPH-BASED TRAFFIC MODELING

Based on the proposal in [6], a traffic situation over n time steps is modeled as a sequence $\mathcal{G}_1, \dots, \mathcal{G}_n$ of graphs centered around a vehicle ν_0 . For a graph $\mathcal{G}_i = (\mathcal{V}_i, \mathcal{E}_i)$, the sets \mathcal{V}_i and \mathcal{E}_i refer to the agents currently in the scene and their edges, respectively. Given an agent $\nu \in \mathcal{V}_i$, the model has access to its historic observations $\mathbf{f}_i^\nu \in \mathbb{R}^{d_f}$, such as previous planar positions and velocities (see Table I) from time $t - t_h$ until t . The graphs within the observation window may be dissimilar at different time instants because of the arrival and departure of agents. Predictions are computed for all the agents \mathcal{V}_t still in the scene at prediction time t . Given the full history

$$\mathcal{H} = \left(\{\mathcal{G}_i\}_{i=t-t_h}^t, \{\{\mathbf{f}_i^\nu\}_{\nu \in \mathcal{V}_i}\}_{i=t-t_h}^t \right) \quad (2)$$

probabilistic trajectory prediction can then be summarized as modeling the conditional distribution

$$p \left(\left\{ \left(\mathbf{x}_{t+1}^\nu, \dots, \mathbf{x}_{t+t_f}^\nu \right) \right\}_{\nu \in \mathcal{V}_t} \middle| \mathcal{H} \right). \quad (3)$$

While the feature histories of different nodes can be of different lengths at the prediction time instant t , the model should still be able to predict the future trajectory for all nodes currently in the graph.

V. MOTION MODELING

The prediction model consists of a deep neural network that learns to predict the inputs $\mathbf{u} = [u_1, u_2]$ of a differentially constrained motion model with states \mathbf{x} . Several motion models used in target tracking [7] and predictive control [8] applications hold potential for use in behavior prediction. This research aims to investigate alternative formulations and draw conclusions regarding their usability and effectiveness. The models considered are of different orders, but they all have at least two state variables $[x, y]$, used to represent the planar positions of the prediction target.

TABLE I
INPUT FEATURES

Feature	Description	Unit
x	Longitudinal coordinate	m
y	Lateral coordinate	m
v_x	Instantaneous longitudinal velocity	m/s
v_y	Instantaneous lateral velocity	m/s
a_x	Instantaneous longitudinal acceleration	m/s ²
a_y	Instantaneous lateral acceleration	m/s ²
ψ	Yaw angle	rad
<i>Highway specific</i> [24]		
d_y	Lateral deviation from the current lane centerline	$[-1, 1]$
d_r	Lateral deviation from the road center	$[-1, 1]$
<i>Roundabout specific</i> [6]		
r	Euclidean distance from the roundabout center	m
θ	Angle relative to the roundabout center	rad

A. Pure Integrators

Pure-integrator models are the simplest considered here. The inputs enter into the differential equations with the highest derivative, which depends on the model degree. Intermediate state transitions are modeled as direct integrations.

1) *Single Integrator (1XI)*: The model has two states (x, y), and their rate of change can be directly controlled by the neural network, i.e., velocities v_x, v_y are control signals u_1, u_2 , respectively as

$$\dot{x} = u_1 \quad (4a)$$

$$\dot{y} = u_2 \quad (4b)$$

2) *Double Integrator (2XI)*: The model has four states, positions and velocities. The accelerations can be controlled by the network:

$$\dot{v}_x = u_1 \quad (5a)$$

$$\dot{v}_y = u_2 \quad (5b)$$

3) *Triple Integrator (3XI)*: The model has the most states (six) of all considered. In this case, the neural network controls the jerk:

$$\dot{a}_x = u_1 \quad (6a)$$

$$\dot{a}_y = u_2 \quad (6b)$$

B. Orientation-Based Models

Orientation-based models refer to motion models with internal states of orientation ψ and speed v , generally formulated as

$$\dot{x} = v \cos(\psi) \quad (7a)$$

$$\dot{y} = v \sin(\psi) \quad (7b)$$

$$\dot{\psi} = \chi(\mathbf{x}, \mathbf{u}) \quad (7c)$$

$$\dot{v} = u_2, \quad (7d)$$

where the driving function χ varies by chosen model, stated explicitly in the respective descriptions.

1) *Curvilinear (CL)*: This refers to a general, curvilinear-motion model [7]:

$$\dot{\psi} = \frac{u_1}{v}, \quad (8)$$

where the input u_1 represents the acceleration perpendicular to the trajectory.

2) *Curvature (CT)*: Mathematically, the curvature formulation looks similar to the curvilinear-motion model. However, the input does not refer to the acceleration but instead the curvature of the current trajectory arc:

$$\dot{\psi} = u_1 v \quad (9)$$

3) *Unicycle (UC)*: The unicycle model represents the vehicle as a single controllable wheel, where the change in turn rate is one of the inputs:

$$\dot{\psi} = u_1 \quad (10)$$

In [4], this is used to describe wheeled vehicles.

4) *Kinematic Single-Track (ST)*: The kinematic single-track model, illustrated in Fig. 1, is commonly used in motion planning and control applications [8]. Here, the orientation is controlled by the steering angle u_1 :

$$\dot{x} = v \cos(\psi + \beta) \quad (11a)$$

$$\dot{y} = v \sin(\psi + \beta) \quad (11b)$$

$$\dot{\psi} = \frac{v}{l_r} \sin(\beta) \quad (11c)$$

$$\beta = \arctan\left(\frac{l_r}{l_f + l_r} \tan(u_1)\right) \quad (11d)$$

In this research, the lengths l_f and l_r that make up the wheelbase are estimated using the current vehicle's dimensions. Note that the angle β enters into the equations describing \dot{x} and \dot{y} , which is different from (7). A slightly modified version of this model is used in [5].

C. Neural Ordinary Differential Equations

A neural ODE is a type of neural network that learns a continuous-time dynamic system by modeling its derivatives [9]. Adopting the methods proposed in our previous work [6], two general neural ODE formulations of varying order are considered. The motion models consist of differentially-constrained feedforward networks with learnable parameters.

1) *First Order (N-ODE1)*: Two separate ODEs, f_1 and f_2 are used to describe the state dynamics where each function is associated with its respective input:

$$\dot{x} = f_1(x, y, u_1) \quad (12a)$$

$$\dot{y} = f_2(x, y, u_2) \quad (12b)$$

2) *Second Order (N-ODE2)*: For the second-order model, only the highest-order derivatives are parameterized. Intermediate states are pure integrators, which gives

$$\dot{x} = v_x \quad (13a)$$

$$\dot{y} = v_y \quad (13b)$$

$$\dot{v}_x = f_1(v_x, v_y, u_1) \quad (13c)$$

$$\dot{v}_y = f_2(v_x, v_y, u_2) \quad (13d)$$

D. Generating Dynamically Feasible Model Inputs

Although the neural network may directly learn which ranges of model inputs are suitable for the best performance, outputting feasible values can not be guaranteed unless explicitly handled. Additionally, bounding the inputs further supports the goal of guaranteeing feasible outputs. Bounds on the motion-model inputs are enforced using the HardTanh activation function:

$$\text{HardTanh}_u(u) = \begin{cases} u_{\max}, & u > u_{\max} \\ u_{\min}, & u < u_{\min} \\ u, & \text{otherwise} \end{cases} \quad (14)$$

Most input bounds are based on the training data, if available; otherwise, they are determined by physical insight. For simplicity, the double-sided constraint is assumed to be symmetric, i.e., $u_{\min} = -u_{\max}$, which is reasonable for all inputs.

E. Numerical Integration

The motion models presented in Section V are all formulated as controllable, continuous-time ODEs. The model states are retrieved by solving an initial-value problem using methods of numerical integration. In this research, how the choice of these methods affects the prediction performance is investigated, most of which are in the Runge-Kutta family of methods [25]. Consider the general model in (1), stated again for convenience:

$$\dot{\mathbf{x}} = f(\mathbf{x}, \mathbf{u}) \quad (15)$$

The perhaps most well-known ODE solver is the forward-Euler method, which for a given step size h is formulated:

$$\mathbf{x}_{k+1} = \mathbf{x}_k + hf(\mathbf{x}_k, \mathbf{u}_k) \quad (16)$$

Due to its simplicity and low computational cost, the forward-Euler method is an appealing choice for solving differential equations. It is also the choice of method in [5]. However, the forward-Euler method does have drawbacks, most notably a small region of stability, heavily dependent on the appropriate choice of step size h [25]. Other methods, specifically those of higher order, are typically favored in practical applications where accuracy is more important. The classic fourth-order Runge-Kutta method is one such example [25]:

$$\eta_1 = f(\mathbf{x}_k, \mathbf{u}_k), \quad (17a)$$

$$\eta_2 = f\left(\mathbf{x}_k + \frac{h}{2}\eta_1, \mathbf{u}_k\right), \quad (17b)$$

$$\eta_3 = f\left(\mathbf{x}_k + \frac{h}{2}\eta_2, \mathbf{u}_k\right), \quad (17c)$$

$$\eta_4 = f(\mathbf{x}_k + h\eta_3, \mathbf{u}_k), \quad (17d)$$

$$\mathbf{x}_{k+1} = \mathbf{x}_k + \frac{h}{6}(\eta_1 + 2\eta_2 + 2\eta_3 + \eta_4) \quad (17e)$$

In numerical analysis software, it is generally not a fixed-step method like those stated in this subsection that is the default. Instead, it is typically a variable-step solver, such as the Dormand-Prince method [26]. In these solvers, the step size h is computed based on intermediate calculations.

VI. TRAJECTORY PREDICTION MODEL

This work leverages the MTP-GO² model presented in our previous research. Therefore, only a brief summary of the main components will be presented here; for details, see [6]. The complete MTP-GO model consists of a GNN-based encoder-decoder module that computes the inputs to a motion model for trajectory forecasting. The output is multi-modal, consisting of several candidate trajectories $\hat{\mathbf{x}}_{t+1}^j, \dots, \hat{\mathbf{x}}_{t+t_f}^j$ for different components $j \in \{1, \dots, M\}$ used to capture different maneuvers. In addition, each candidate is accompanied by a predicted state covariance $\mathbf{P}_{t+1}^j, \dots, \mathbf{P}_{t+t_f}^j$ which is estimated using an Extended Kalman Filter (EKF).

A. Temporal Graph Neural Network Encoder

1) *Graph-Gated Recurrent Unit*: Using an extended Gated Recurrent Unit (GRU) cell [27] where the conventional linear mappings are replaced by GNN components [28], spatial-temporal interactions can be captured. The GNNs takes as input the representations for the specific node ν and the information of other nodes in the graph. Intermediate representations are computed by two GNNs as

$$[\boldsymbol{\kappa}_{r,i}^\nu \parallel \boldsymbol{\kappa}_{z,i}^\nu \parallel \boldsymbol{\kappa}_{h,i}^\nu] = \text{GNN}_f\left(\mathbf{f}_i^\nu, \{\mathbf{f}_\nu^\tau\}_{\tau \neq \nu}\right) \quad (18a)$$

$$[\boldsymbol{\xi}_{r,i}^\nu \parallel \boldsymbol{\xi}_{z,i}^\nu \parallel \boldsymbol{\xi}_{h,i}^\nu] = \text{GNN}_h\left(\mathbf{h}_{i-1}^\nu, \{\mathbf{h}_{i-1}^\tau\}_{\tau \neq \nu}\right), \quad (18b)$$

where \parallel is the concatenation operation. These are then used to compute the representation \mathbf{h}_i^ν for time step i as

$$\mathbf{r}_i^\nu = \sigma(\boldsymbol{\kappa}_{r,i}^\nu + \boldsymbol{\xi}_{r,i}^\nu + \mathbf{b}_r) \quad (19a)$$

$$\mathbf{z}_i^\nu = \sigma(\boldsymbol{\kappa}_{z,i}^\nu + \boldsymbol{\xi}_{z,i}^\nu + \mathbf{b}_z) \quad (19b)$$

$$\tilde{\mathbf{h}}_i^\nu = \phi(\boldsymbol{\kappa}_{h,i}^\nu + \mathbf{r}_i^\nu \odot \boldsymbol{\xi}_{h,i}^\nu + \mathbf{b}_h) \quad (19c)$$

$$\mathbf{h}_i^\nu = (\mathbf{1} - \mathbf{z}_i^\nu) \odot \tilde{\mathbf{h}}_i^\nu + \mathbf{z}_i^\nu \odot \mathbf{h}_{i-1}^\nu, \quad (19d)$$

where the bias terms $\mathbf{b}_r, \mathbf{b}_z, \mathbf{b}_h \in \mathbb{R}^{d_h}$ are additional learnable parameters, \odot the Hadamard product, σ the sigmoid function, and ϕ is the hyperbolic tangent.

2) *Graph Neural Network*: In [6], the properties of different GNN layers and their use in trajectory prediction are investigated. Here, the GNNs in (18) are modeled using a modified version of the Graph Attention Network (GAT) [29] framework. To compute the aggregation of weights for a neighborhood, GAT layers utilize an attention mechanism [30]. In our modified version, called *GAT+*, the results of the standard GAT output are summed with the output of a linear layer that takes the representation of the center node [6].

B. Decoder with Temporal Attention Mechanism

Similarly to the encoder, the decoder also utilizes a graph-GRU component. Its task is to compute the motion model input \mathbf{u} and the process noise \mathbf{Q} for time steps $t+1, \dots, t+t_f$. The first \mathbf{h} -input to the decoder is taken as the last hidden representation from the encoder \mathbf{h}_t^ν . The updates then proceed just as in (18b). To construct the input \mathbf{f} , the decoder additionally utilizes a temporal attention mechanism conditioned on the full encoder representation $\mathbf{o}_t^\nu = [\mathbf{h}_{t-t_h}^\nu, \dots, \mathbf{h}_t^\nu]$.

²Multi-agent Trajectory Prediction by Graph-enhanced neural ODEs

C. Uncertainty Propagation in Forecasting

The prediction step of the EKF is used to estimate the future states and state covariances. Combining the computed estimates with a mixture density network [31], the model outputs multimodal future predictions by learning the parameters of a Gaussian mixture model [31].

1) *Extended Kalman Filter*: For a differentiable state-transition function f , the prediction step of the EKF is:

$$\hat{\mathbf{x}}_{k+1} = f(\hat{\mathbf{x}}_{k|k}, \mathbf{u}_k) \quad (20a)$$

$$\mathbf{P}_{k+1} = \mathbf{F}_k \mathbf{P}_{k|k} \mathbf{F}_k^T + \mathbf{G}_k \mathbf{Q}_{k|k} \mathbf{G}_k^T, \quad (20b)$$

where

$$\mathbf{F}_k = \left. \frac{\partial f}{\partial \mathbf{x}} \right|_{\hat{\mathbf{x}}_{k|k}, \mathbf{u}_k} \quad (21)$$

Here, $\hat{\mathbf{x}}$ and \mathbf{P} refer to the state estimate and state covariance estimate, respectively, and f is the current motion model. For all motion models, the process noise is assumed to be a consequence of the predicted inputs and therefore enters into the two highest-order states. This noise is modeled as zero-mean with covariance matrix

$$\mathbf{Q} = \begin{pmatrix} \sigma_1^2 & \rho\sigma_1\sigma_2 \\ \rho\sigma_1\sigma_2 & \sigma_2^2 \end{pmatrix} \quad (22)$$

Assuming that the noise is additive, \mathbf{G}_k is designed as a matrix of constants. In the simplest case with two state variables, then $\mathbf{G}_k = T_s \cdot \mathbf{I}_2$, where T_s is the sample period. For higher-order state-space models, \mathbf{G}_k is generalized:

$$\mathbf{G}_k = T_s \begin{pmatrix} 0 & \dots & 1 & 0 \\ 0 & \dots & 0 & 1 \end{pmatrix}^T \quad (23)$$

2) *Mixture Density Network*: Each output vector \mathbf{y}_k of the model contains mixing coefficients $\boldsymbol{\pi}^j$, along with the state estimate $\hat{\mathbf{x}}_k^j$ and state covariance estimate \mathbf{P}_k^j for all mixtures $j \in \{1, \dots, M\}$:

$$\mathbf{y}_k = \left(\boldsymbol{\pi}^j, \{ \hat{\mathbf{x}}_k^j, \mathbf{P}_k^j \}_{j=1}^M \right), \quad (24)$$

where $\boldsymbol{\pi}^j$ is constant over the prediction horizon t_f . For notational convenience, the predictions are indexed from $k = 1, \dots, t_f$. The model is trained by minimizing the Negative Log-Likelihood (NLL) of the ground truth trajectory

$$\mathcal{L}_{\text{NLL}} = \sum_{k=1}^{t_f} -\log \left(\sum_j \boldsymbol{\pi}^j \mathcal{N}(\mathbf{x}_k | \hat{\mathbf{x}}_k^j, \mathbf{P}_k^j) \right) \quad (25)$$

VII. EVALUATION & RESULTS

The model combinations are evaluated using different data sets, encouraged by their varying dynamics and behavior. To motivate the use of a deep-learning-based backbone to compute the motion model inputs, a Constant Acceleration (CA) and Constant Velocity (CV) model is included as a reference. Unless stated differently, the classic fourth-order Runge-Kutta method (RK4) was used as the numerical solver. For explicit methods, the solver step size h was set to the sample period $T_s = 0.2$. In Section VII-D, the different model combinations are evaluated on different data sets. A study on numerical solver implications is presented in Section VII-E.

A. Data Sets

For training and testing, two different data sets, *highD* [10] and *rounD* [11], were used. The data sets contain recorded trajectories from different locations in Germany, including various highways and roundabouts. The data contain several hours of naturalistic driving data captured at 25 Hz. Observations for training and inference cover at most 3 s and at least one sample. During the preprocessing stage, the original input and target data were down-sampled by a factor of 5, effectively setting the sampling period $T_s = 0.2$ s.

B. Training and Implementation Details

All implementations were done using PyTorch [32] and PyTorch Geometric [33]. For numerical integration, we used `torchdiffeq` [34]. Jacobian calculations were performed using `functorch` [35]. The *Adam* optimizer [36] was employed with a batch size of 128 and a learning rate of 0.0001. A key observation revealed that the number of ground truth states used during training substantially affected test performance. For instance, with motion models containing four states, $[x, y, v, \psi]$, despite the dependency of x and y on v , having the model concurrently learn to enhance all three as opposed to only x and y led to a notable performance improvement. It is important to note that the orientation angle cannot be directly incorporated in (25) as it fails to account for the cyclical nature of angles.

C. Evaluation Metrics

Several metrics are used to evaluate the investigated model combinations, which are presented here for a single agent. These are then averaged over all agents in all traffic situations in the test set. As the predicted distribution is a mixture, L^2 -based metrics are computed using the component j^* with the predicted largest weight, $j^* = \operatorname{argmax}_j \boldsymbol{\pi}^j$.

- *Average Displacement Error (ADE)*:

$$\text{ADE} = \frac{1}{t_f} \sum_{k=1}^{t_f} \|\hat{\mathbf{x}}_k - \mathbf{x}_k\|_2 \quad (26)$$

- *Final Displacement Error (FDE)*:

$$\text{FDE} = \|\hat{\mathbf{x}}_{t_f} - \mathbf{x}_{t_f}\|_2 \quad (27)$$

- *Miss Rate (MR)*: The ratio of cases where the predicted final position is not within 2 m of the ground truth [2].

- *Average Path Displacement Error (APDE)*:

$$\text{APDE} = \frac{1}{t_f} \sum_{k=1}^{t_f} \|\hat{\mathbf{x}}_k - \mathbf{x}_{k^*}\|_2 \quad (28)$$

$$k^* = \operatorname{argmin}_i \|\hat{\mathbf{x}}_k - \mathbf{x}_i\|_2$$

- *Average Negative Log-Likelihood (ANLL)*:

$$\text{ANLL} = \frac{1}{t_f} \sum_{k=1}^{t_f} -\log \left(\sum_j \boldsymbol{\pi}^j \mathcal{N}(\mathbf{x}_k | \hat{\mathbf{x}}_k^j, \mathbf{P}_k^j) \right) \quad (29)$$

- *Final Negative Log-Likelihood (FNLL)*:

$$\text{FNLL} = -\log \left(\sum_j \boldsymbol{\pi}^j \mathcal{N}(\mathbf{x}_{t_f} | \hat{\mathbf{x}}_{t_f}^j, \mathbf{P}_{t_f}^j) \right) \quad (30)$$

TABLE II
MODEL COMBINATION PERFORMANCE BY DATA SET

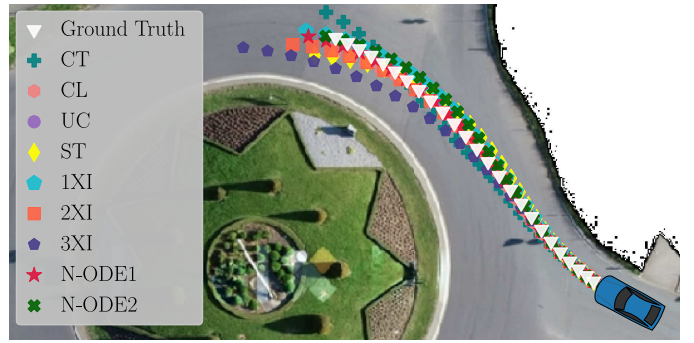
Data set	Model	ADE	FDE	MR	APDE	ANLL	FNLL
<i>highD</i>	CA	0.78	2.63	0.55	0.46	—	—
	CV	1.49	4.01	0.79	0.87	—	—
	1XI	0.25	0.85	0.05	0.25	-1.74	1.27
	2XI	0.28	0.92	0.05	0.28	-1.72	1.57
	3XI	0.32	1.05	0.06	0.31	4.95	4.30
	CL	0.32	1.01	0.06	0.31	-0.68	1.99
	CT	0.33	1.02	0.07	0.31	-0.76	1.97
	UC	0.28	0.92	0.06	0.27	-0.84	1.77
	ST	0.28	0.93	0.06	0.27	-0.80	1.78
	N-ODE1	0.26	0.89	0.06	0.25	-2.03	1.32
	N-ODE2	0.27	0.91	0.06	0.26	-1.90	1.34
<i>roundD</i>	CA	4.83	16.2	0.95	3.90	—	—
	CV	6.49	17.1	0.94	4.25	—	—
	1XI	0.99	3.03	0.34	0.60	0.16	3.31
	2XI	0.99	3.10	0.36	0.61	-0.17	3.83
	3XI	1.45	4.54	0.57	0.96	0.67	4.88
	CL	1.48	4.81	0.65	1.10	1.22	4.81
	CT	1.38	4.04	0.74	0.98	0.94	4.40
	UC	1.29	3.85	0.57	0.90	0.93	4.48
	ST	1.24	3.67	0.56	0.85	0.68	4.01
	N-ODE1	0.99	3.07	0.37	0.63	0.20	3.38
	N-ODE2	0.98	3.09	0.35	0.63	-0.19	3.75

D. Evaluation of Model Combinations

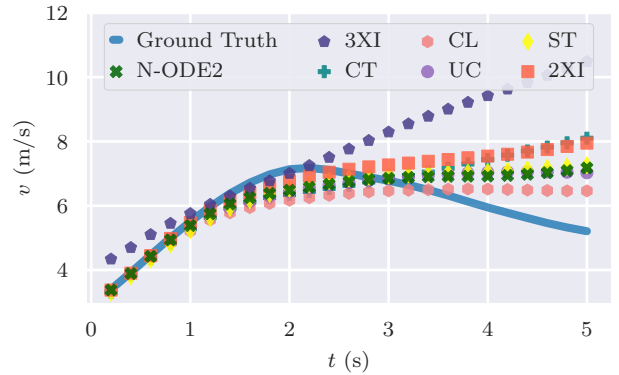
The prediction model’s performance using different motion models on the two data sets is presented in Table II.

1) *Highway*: There is no significant difference between the employed motion models for the highway trajectory prediction task, with most methods being comparable to the first decimal on L^2 -based metrics. However, some minor differences indicate that the 3XI model, along with all the orientation-based models, performs slightly worse than the others, particularly on NLL. This is interesting, especially considering that highway trajectories are typically smooth, often described using quintic polynomials in motion planning applications [37]. By that argument, the 3XI model should intuitively be competitive to the other methods in this context, which is not the case. Instead, it is the models 1XI, 2XI, N-ODE1, and N-ODE2 that report the best results combined over all metrics.

2) *Roundabout*: The performance of the methods when predicting roundabout trajectories, compared to the results for highway predictions, indicates that this is a more complex problem. Regardless, most of the deep-learning enhanced motion models perform well. The orientation-based models are underperforming in this context, reporting errors significantly larger than the others. This is interesting, given that these types of motion models are typically used in related works [3]–[5]. Instead, the combined results indicate that simple integrators are adequate for accurate learning-based motion prediction, which is encouraging given their reduced complexity and low computational demands. The prediction performance can be further assessed by studying the illustration in Fig. 2, showing an example prediction using test data from the *roundD* data set. In particular, Fig. 2b illustrates the difficulties of the investigated problem, but also the limitations of the methods. Over a 5 s prediction horizon, numerous events can occur, and although the methods accurately capture the overall true



(a) While the method is capable of multi-agent predictions, the blue car illustrates a single forecast objective. The quality of the prediction between motion models varies slightly, although most predictions are close to the ground truth. The 1XI, N-ODE1, and N-ODE2 models are visually the best performing in this scenario. The figure background is from the *roundD* data set [11].



(b) It is clear from the predictions in (a) that most methods overshoot the true trajectory. Comparing how well the model predicts the velocity may provide an indication of which models are the most effective.

Fig. 2. Example predictions of the motion models on a roundabout scenario.

path, only a few successfully predict deceleration entering the curve. Still, most models remain accurate for up to 3 s before diverging.

E. Implications of Numerical Solver Selection

Since the choice of integration method could substantially impact the solution trajectory, it is interesting to study its effect within this context. Three different motion models were selected for this study: ST, 2XI, and N-ODE2. The models were trained and evaluated using different numerical solvers: forward-Euler method (EF), Heun’s method (Heun), Kutta’s third-order method (RK3), classic fourth-order Runge-Kutta method (RK4), Dormand-Prince variable-step method (DOPRI), and an implicit-Adams method (Adams) [25]. Both data sets were subjected to the investigation but yielded similar results. While the conclusions hold for both scenarios, only the performance on *roundD* will be discussed here.

The effect of numerical solver selection is presented in Table III. The results illustrate varying model responses to different solvers. What is true for all motion models, however, is that the worst results are achieved in combination with EF. Interestingly, using a second-order solver, like Heun’s, has a significant positive impact on performance compared

TABLE III
ROUND SOLVER PERFORMANCE

Model	Solver	ADE	FDE	MR	APDE	ANLL	FNLL
ST	EF	1.82	4.97	0.73	1.24	2.32	4.71
	Heun	1.23	3.64	0.55	0.83	0.74	4.10
	RK3	1.28	3.80	0.58	0.87	0.75	4.12
	RK4	1.24	3.67	0.56	0.85	0.68	4.01
	DOPRI	1.30	3.84	0.67	0.90	0.91	4.42
	Adams	1.24	3.69	0.56	0.84	0.73	4.12
2XI	EF	1.50	4.18	0.58	0.89	5.67	7.10
	Heun	0.97	3.07	0.34	0.60	-0.22	3.75
	RK3	0.98	3.08	0.35	0.61	-0.22	3.77
	RK4	0.99	3.10	0.36	0.61	-0.17	3.83
	DOPRI	0.99	3.09	0.36	0.60	-0.19	3.77
	Adams	1.01	3.12	0.39	0.61	-0.17	3.73
N-ODE2	EF	1.90	7.48	0.72	1.07	5.84	7.48
	Heun	1.00	3.11	0.35	0.62	-0.19	3.76
	RK3	0.99	3.10	0.37	0.62	-0.19	3.77
	RK4	0.98	3.09	0.35	0.63	-0.19	3.75
	DOPRI	1.10	3.46	0.44	0.70	0.24	4.08
	Adams	0.98	3.04	0.35	0.61	-0.19	3.73

to EF. Going beyond the second-order method, offers only marginal performance increases, much of which is dependent on the model–solver combination. For example, N-ODE2 responded positively toward using the implicit Adam’s method, but arguably not enough to be considered significant.

The trade-off between performance and computational demands is an interesting topic. In Fig. 3, the training performance over 10 hours using the aforementioned models and selected solvers is presented. The choice of numerical solver can have a significant impact on the training duration, likely resulting from additional function evaluations specific to higher-order methods. As one might expect, employing the variable-step solver DOPRI led to a notably extended training duration.

Although the effect on model inference time is not as pronounced as in the case of training performance, similar trends can be observed (see Fig. 4). Most model-solver combinations require less than 1 millisecond to compute predictions for a single agent, with little variation. However, as with the training duration, using the variable-step solver DOPRI necessitated a much longer computation time.

VIII. CONCLUSION

An evaluation of differentially-constrained motion models and numerical solvers for learning-based trajectory prediction was presented. Using the MTP-GO framework, a range of motion models, from pure integrators to kinematic models and neural ODEs, were examined. It was found that simpler models, such as low-order integrators, yielded the best results irrespective of scenario complexity. The study also revealed that the selection of a numerical solver can significantly influence both training and prediction performance. Although the findings indicate that effective prediction performance can be achieved using a second-order numerical solver like Heun’s method, it underscores the importance of making well-informed model and solver choices when implementing these methods.

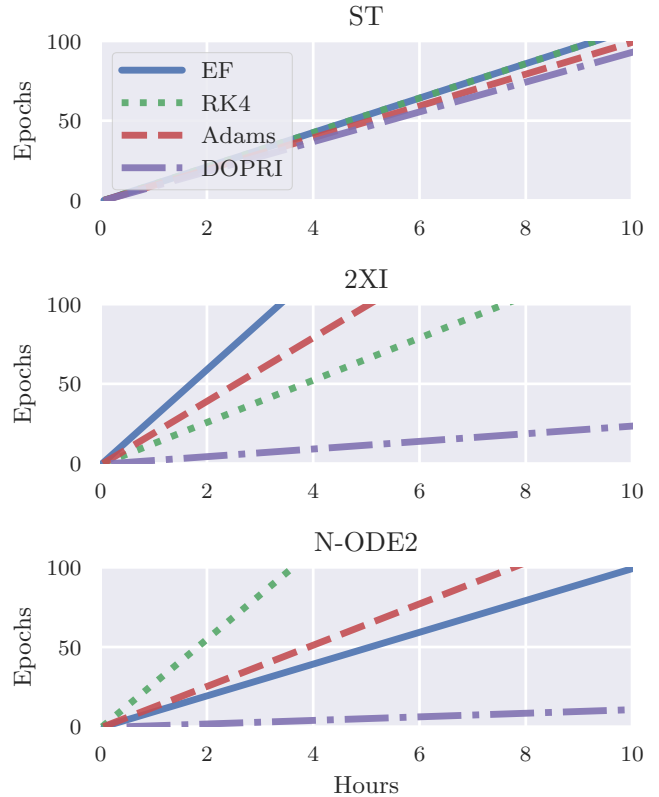


Fig. 3. Training progress of ST, 2XI, and N-ODE2 over 100 epochs for different solvers on the *round* data set, using one NVIDIA A100 GPU. The training process for the various models is differently affected by solver selection, especially when using the variable-step solver, DOPRI. Interestingly, training N-ODE2 with EF resulted in a longer total duration than using RK4. This is possibly because of the combination of the small stability region of EFs and the N-ODE2s dynamics. Instead the additional function evaluations RK4 adds increased stability during training. Although excluded from the figure for clarity, solvers like Heun’s and RK3 were in magnitudes similar to EF.

ACKNOWLEDGMENTS

Computations were enabled by the supercomputing resource Berzelius provided by National Supercomputer Centre at Linköping University and the Knut and Alice Wallenberg foundation.

REFERENCES

- [1] S. Mozaffari, O. Y. Al-Jarrah, M. Dianati, P. Jennings, and A. Mouzakitis, “Deep learning-based vehicle behavior prediction for autonomous driving applications: A review,” *IEEE Transactions on Intelligent Transportation Systems*, 2020.
- [2] Y. Huang, J. Du, Z. Yang, Z. Zhou, L. Zhang, and H. Chen, “A survey on trajectory-prediction methods for autonomous driving,” *IEEE Transactions on Intelligent Vehicles*, 2022.
- [3] H. Cui, T. Nguyen, F.-C. Chou, T.-H. Lin, J. Schneider, D. Bradley, and N. Djuric, “Deep kinematic models for kinematically feasible vehicle trajectory predictions,” in *2020 IEEE International Conference on Robotics and Automation (ICRA)*, 2020, pp. 10 563–10 569.
- [4] T. Salzmann, B. Ivanovic, P. Chakravarty, and M. Pavone, “Trajectron++: Dynamically-feasible trajectory forecasting with heterogeneous data,” in *European Conference on Computer Vision*. Springer, 2020, pp. 683–700.
- [5] J. Li, H. Ma, Z. Zhang, J. Li, and M. Tomizuka, “Spatio-temporal graph dual-attention network for multi-agent prediction and tracking,” *IEEE Transactions on Intelligent Transportation Systems*, vol. 23, no. 8, pp. 10 556–10 569, 2022.

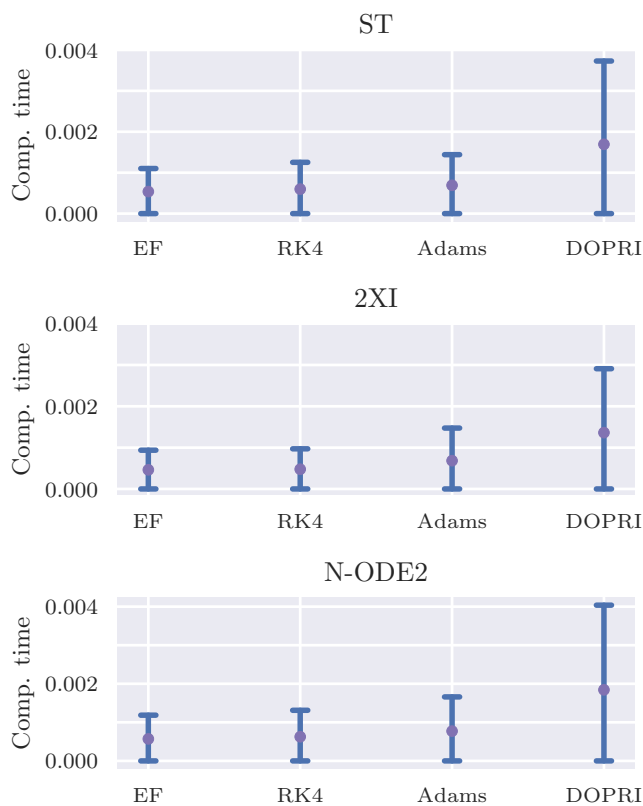


Fig. 4. Inference time per forecast objective using ST, 2XI, and N-ODE2 with different solvers on the *round* test set, using a single NVIDIA A100 GPU. The data points (graph sequences) consist of a varying number of agents, leading to variability in computation time. To represent this variation, a 95% confidence interval is employed.

[6] T. Westny, J. Oskarsson, B. Olofsson, and E. Frisk, "MTP-GO: Graph-based probabilistic multi-agent trajectory prediction with neural ODEs," *arXiv preprint arXiv:2302.00735*, 2023.

[7] X. R. Li and V. P. Jilkov, "Survey of maneuvering target tracking. Part I. Dynamic models," *IEEE Transactions on Aerospace and Electronic Systems*, vol. 39, no. 4, pp. 1333–1364, 2003.

[8] B. Paden, M. Čáp, S. Z. Yong, D. Yershov, and E. Frazzoli, "A survey of motion planning and control techniques for self-driving urban vehicles," *IEEE Transactions on Intelligent Vehicles*, vol. 1, no. 1, pp. 33–55, 2016.

[9] R. T. Q. Chen, Y. Rubanova, J. Bettencourt, and D. K. Duvenaud, "Neural ordinary differential equations," in *Advances in Neural Information Processing Systems*, vol. 31, 2018.

[10] R. Krajewski, J. Bock, L. Kloecker, and L. Eckstein, "The highD dataset: A drone dataset of naturalistic vehicle trajectories on german highways for validation of highly automated driving systems," in *21st International Conference on Intelligent Transportation Systems (ITSC)*. IEEE, 2018, pp. 2118–2125.

[11] R. Krajewski, T. Moers, J. Bock, L. Vater, and L. Eckstein, "The round dataset: A drone dataset of road user trajectories at roundabouts in germany," in *23rd International Conference on Intelligent Transportation Systems (ITSC)*. IEEE, 2020.

[12] C.-F. Lin, A. G. Ulsoy, and D. J. LeBlanc, "Vehicle dynamics and external disturbance estimation for vehicle path prediction," *IEEE Transactions on Control Systems Technology*, vol. 8, no. 3, pp. 508–518, 2000.

[13] A. Polychronopoulos, M. Tsogas, A. J. Amditis, and L. Andreone, "Sensor fusion for predicting vehicles' path for collision avoidance systems," *IEEE Transactions on Intelligent Transportation Systems*, vol. 8, no. 3, pp. 549–562, 2007.

[14] R. Schubert, E. Richter, and G. Wanielik, "Comparison and evaluation of advanced motion models for vehicle tracking," in *11th International Conference on Information Fusion*. IEEE, 2008.

[15] A. Kullberg, I. Skog, and G. Hendeby, "Online joint state inference and learning of partially unknown state-space models," *IEEE Transactions on Signal Processing*, vol. 69, pp. 4149–4161, 2021.

[16] Y. Hu, W. Zhan, and M. Tomizuka, "Probabilistic prediction of vehicle semantic intention and motion," in *IEEE Intelligent Vehicles Symposium (IV)*, 2018, pp. 307–313.

[17] K. Messaoud, I. Yahiaoui, A. Verroust-Blondet, and F. Nashashibi, "Attention based vehicle trajectory prediction," *IEEE Transactions on Intelligent Vehicles*, vol. 6, no. 1, pp. 175–185, 2021.

[18] N. Deo and M. M. Trivedi, "Convolutional social pooling for vehicle trajectory prediction," in *Proceedings of the IEEE Conference on Computer Vision and Pattern Recognition Workshops*, 2018.

[19] X. Li, X. Ying, and M. C. Chuah, "GRIP++: Enhanced graph-based interaction-aware trajectory prediction for autonomous driving," *arXiv preprint arXiv:1907.07792*, 2019.

[20] Y. Liu, J. Zhang, L. Fang, Q. Jiang, and B. Zhou, "Multimodal motion prediction with stacked transformers," in *Proceedings of the IEEE/CVF Conference on Computer Vision and Pattern Recognition*, 2021, pp. 7577–7586.

[21] Z. Huang, X. Mo, and C. Lv, "Multi-modal motion prediction with transformer-based neural network for autonomous driving," in *2022 International Conference on Robotics and Automation (ICRA)*. IEEE, 2022, pp. 2605–2611.

[22] H. Jeon, J. Choi, and D. Kum, "SCALE-Net: Scalable vehicle trajectory prediction network under random number of interacting vehicles via edge-enhanced graph convolutional neural network," in *2020 IEEE/RSJ International Conference on Intelligent Robots and Systems (IROS)*, 2020, pp. 2095–2102.

[23] Y. Hu, W. Zhan, and M. Tomizuka, "Scenario-transferable semantic graph reasoning for interaction-aware probabilistic prediction," *IEEE Transactions on Intelligent Transportation Systems*, vol. 23, no. 12, pp. 23 212–23 230, 2022.

[24] T. Westny, E. Frisk, and B. Olofsson, "Vehicle behavior prediction and generalization using imbalanced learning techniques," in *IEEE 24th International Conference on Intelligent Transportation Systems (ITSC)*, 2021, pp. 2003–2010.

[25] U. M. Ascher and L. R. Petzold, *Computer methods for ordinary differential equations and differential-algebraic equations*. SIAM, 1998, vol. 61.

[26] J. R. Dormand and P. J. Prince, "A family of embedded Runge-Kutta formulae," *Journal of Computational and Applied Mathematics*, vol. 6, no. 1, pp. 19–26, 1980.

[27] K. Cho, B. van Merriënboer, D. Bahdanau, and Y. Bengio, "On the properties of neural machine translation: Encoder–decoder approaches," in *Proceedings of SSST-8, Eighth Workshop on Syntax, Semantics and Structure in Statistical Translation*, 2014, pp. 103–111.

[28] J. Oskarsson, P. Sidén, and F. Lindsten, "Temporal graph neural networks for irregular data," in *Proceedings of The 26th International Conference on Artificial Intelligence and Statistics*, 2023.

[29] S. Brody, U. Alon, and E. Yahav, "How attentive are graph attention networks?" in *International Conference on Learning Representations (ICLR)*, 2022.

[30] A. Vaswani, N. Shazeer, N. Parmar, J. Uszkoreit, L. Jones, A. N. Gomez, L. u. Kaiser, and I. Polosukhin, "Attention is all you need," in *Advances in Neural Information Processing Systems*, vol. 30, 2017.

[31] C. M. Bishop, *Pattern recognition and machine learning*. Springer, 2006.

[32] A. Paszke, S. Gross, F. Massa, A. Lerer, J. Bradbury, G. Chanan, T. Killeen, Z. Lin, N. Gimelshein, L. Antiga *et al.*, "Pytorch: An imperative style, high-performance deep learning library," *Advances in neural information processing systems*, vol. 32, 2019.

[33] M. Fey and J. E. Lenssen, "Fast graph representation learning with PyTorch Geometric," in *ICLR Workshop on Representation Learning on Graphs and Manifolds*, 2019.

[34] R. T. Q. Chen, "torchdiffeq," 2018, accessed on 1.09.2022. [Online]. Available: <https://github.com/rtqichen/torchdiffeq>

[35] R. Z. Horace He, "functorch: Jax-like composable function transforms for pytorch," 2021, accessed on 23.11.2022. [Online]. Available: <https://github.com/pytorch/functorch>

[36] D. P. Kingma and J. Ba, "Adam: A Method for Stochastic Optimization," in *International Conference on Learning Representations (ICLR)*, 2015.

[37] M. Werling, S. Kammel, J. Ziegler, and L. Gröll, "Optimal trajectories for time-critical street scenarios using discretized terminal manifolds," *The International Journal of Robotics Research*, vol. 31, no. 3, pp. 346–359, 2012.